Improved Adaptive Robust Control With MRAS for High-Temperature Wound Rotor Synchronous Machine Featuring Anodized Aluminum Coils

Riyad Jbayli, Younes Azzoug, Romain Cousseau, Remus Pusca, Raphael Romary

IEEE Access
Multidisciplinary | Rapid Review | Open Access Journal

Received 15 October 2025, accepted 4 November 2025,
date of publication 7 November 2025, date of current version 13 November 2025.

Digital Object Identifier 10.1109/ACCESS.2025.3630268

RESEARCH ARTICLE

Improved Adaptive Robust Control With MRAS for High-Temperature Wound Rotor Synchronous Machine Featuring Anodized Aluminum Coils

RIYAD JBAYLI, YOUNES AZZOUG, ROMAIN COUSSEAU, REMUS PUSCA, (Member, IEEE), AND RAPHAEL ROMARY, (Member, IEEE)
Univ. Artois, UR 4025, Laboratoire Systèmes Électrotechniques et Environnement (LSEE), F-62400 Béthune, France
Corresponding author: Riyad Jbayli (riyad.jbayli@univ-artois.fr)

ABSTRACT This paper presents a robust and adaptive control strategy for wound rotor synchronous machines with anodized aluminum tape coils, designed to operate reliably at temperatures around 300°C. At such high temperatures, significant changes occur in key motor parameters, including resistance, inductance, and flux linkage. These variations adversely affect the accuracy and stability of speed and current control, making traditional control methods insufficient. To address the challenge, the proposed approach combines cascaded control loops with advanced parameter estimation techniques. Leveraging adaptive algorithms, the system dynamically and continuously estimates and compensates the variations in resistance, inductance, and rotor flux, thereby ensuring accurate control of stator currents and rotor speed. On top of that, the strategy integrates a disturbance observer to detect external perturbations and adjust control actions in real time, improving the overall robustness of the machine under varying operating conditions. Simulation and experimental results confirm the effectiveness of the proposed adaptive robust control strategy, demonstrating improved performance and stability of the wound rotor synchronous machine even under extreme thermal operating conditions.

INDEX TERMS Wound rotor synchronous machine, anodized aluminum tape, disturbance observer, model reference adaptive system, adaptive robust control, high temperature.

I. INTRODUCTION

The increasing need for efficient, reliable, and high-performance electric machines in various fields like industrial automation, transportation, and renewable energy has driven significant attention toward Wound Rotor Synchronous Machines (WRSM). These machines are distinguished by their high torque, compact design, and precise control capabilities [1]. Compared to Permanent Magnet Synchronous Machines (PMSM), WRSM with anodized aluminum tape can operate at much higher rotor temperatures [2]. The choice of winding material plays a key role in improving machine efficiency. Aluminum is an effective alternative to copper, offering lower cost, reduced weight, and good thermal conductivity. Replacing copper by aluminum wires in stator coils can lead to a 50% reduction in total mass [3]. Aluminum has also shown strong performance in applications requiring high speed or frequency [4], [5], introducing challenges for conventional control methods such as Field Oriented Control (FOC). At high temperatures, the coil resistance rises significantly [6], [7], and the rotor flux decreases due to reduced excitation current under constant voltage. These parameter changes negatively affect motor performance, as observed in [8] where these variations disrupt the transfer function and reduce the effectiveness of PI controllers.

To address these challenges, several advanced control strategies have been investigated to enhance the reliability of synchronous machines operating under varying conditions. Techniques like sliding mode control [9], Continuous Time

The associate editor coordinating the review of this manuscript and approving it for publication was Jinquan Xu.

Model Predictive Control (CTMPC) [10], and backstepping control [11] have proven effective in handling changes in machine parameters and external disturbances. These methods adjust the control parameters in real-time, boosting the system's ability to manage uncertainties. In addition, more advanced techniques such as μ-synthesis control [12] and H_∞ control [13] enhance the system stability, especially when facing large disturbances. However, these methods often suffer from practical limitations, including conservatism in H_∞ design, chattering effects in sliding mode control, and high computational complexity in μ-synthesis making their implementation challenging in real-time applications. Another method, Disturbance Observer-Based Control (DOBC) [14], [15], [16], helps to identify disturbances arising from parameters variation.

Despite significant advancements, synchronous machines continue to encounter performance limitations in high-temperature environments, where motor parameters change. In such temperatures, conventional control methods often fail to ensure optimal regulation, particularly in maintaining precise stator current control. To overcome this issue, advanced control methodologies with enhanced adaptability and dynamic response capabilities have been proposed like the Internal Model Control (IMC) [17], Sliding Mode Control [18], Model-Free Predictive Current Control (MFPCC) [19], [20], [21], and Adaptive Robust Control (ARC) [16], [22], [23]. These techniques are specifically designed to estimate and mitigate the adverse effects of parameter fluctuations. While IMC and MFPCC use model-based frameworks for disturbance rejection, ARC offers a more resilient and flexible approach by continuously adapting the control face to variations in stator resistance, inductance, and rotor flux linkage.

Reliable parameter estimation is essential to achieve a successful adaptive control, especially in high-temperature environments where parameters variations become more significant. Techniques like Recursive Least Squares (RLS) [24], Extended Kalman Filter (EKF) [25], and projection-based adaptation [26] are widely used to track motor parameters in real time. While Recursive Least Squares (RLS) and Extended Kalman Filter (EKF) are effective for real-time parameter estimation, they suffer from limitations such as sensitivity to noise, slow convergence in non-ideal conditions, and high computational complexity, especially for large parameter sets. Projection-based adaptation, on the other hand, may face convergence issues and is highly dependent on proper initialization, with a risk of divergence in certain dynamic conditions. Model Reference Adaptive Systems (MRAS) [27], [28], [29], [30], [31] which use stability techniques based on Popov and Lyapunov's lemmas [32], [33] offer a robust alternative that overcomes these challenges by providing better stability and performance in uncertain environments. Employing the Popov and Lyapunov criteria in MRAS guarantees that both the parameter-estimation error and the output-tracking error between the plant and the adjustable model converge to zero [32]. The methods mentioned above for speed and current regulation and for parameters estimation are summarized in Table 1, together with their key advantages and weaknesses.

In [34], a Model-Reference Adaptive System (MRAS) was combined with Adaptive Robust Control (ARC) for PMSM current regulation; simulation results were reported. In [35], the same MRAS–ARC approach was transferred to a WRSM, with simulations only.

In this study, the ARC current controller is advanced by substituting the conventional projection-based adaptation with a Model Reference Adaptive System (MRAS), enabling real-time, temperature-dependent estimation of resistance, inductance and rotor flux from measured voltages, currents, and rotor speed. Speed regulation is achieved by a disturbance observer (DOBC). The method is evaluated in simulation and experiment from ambient to above 290°C, where parameter changes are pronounced. For comparison, an Internal Model Control (IMC) strategy [8] as a robust control and a classical FOC with fixed PI gains [36] are used in all the tests. In FOC, the PI gains are set from nominal parameters and kept fixed, so temperature changes are not compensated. The novelty lies in the integration of MRAS into ARC for variable-speed operation of WRSMs with anodized aluminum windings and validating the full MRAS–ARC–DOBC architecture at high temperature, with a Lyapunov-based stability argument. The aim is to improve transient behavior and to reduce current and speed ripple and THD especially at high temperature by using accurate, temperature aware parameter assessment from MRAS. As summarized in Table 1, DOBC enhances load-step recovery and rejects matched disturbances, MRAS supplies online temperature-aware estimation of machine parameters supported by Popov theory, and ARC uses these estimated parameters with a robust term to keep low current ripple at high temperatures.

This paper is organized as follows: Section II presents the WRSM equations, Sections III and IV discuss DOBC for speed control and MRAS for parameter estimation, Section V outlines the ARC method for current control, and Sections VI and VII provide simulation and experimental results. In section VIII, the conclusion of the paper provides a discussion about the key findings.

II. WRSM'S ANALYTICAL MODEL

The wound rotor synchronous machine is described in the (d, q) reference using the following equations [1]:

$$u_d = R_s i_d + L_d \frac{di_d}{dt} - \omega L_q i_q \tag{1}$$

$$u_q = R_s i_q + L_q \frac{di_q}{dt} + \omega \left(L_d i_d + L_m i_r\right) \tag{2}$$

$$T_e = \frac{3}{2} n_p L_m i_r i_q \tag{3}$$

$$T_e - T_l = J \frac{d\Omega}{dt} + f_c \Omega \tag{4}$$

$$\omega = n_p \Omega \tag{5}$$

$$V_r = R_r i_r \tag{6}$$

TABLE 1. Summary of some related work.

Method	Ref.	Advantages	Weaknesses
Speed control			
DOBC *(used)*	[16]	Improves load-step recovery. Compensates matched disturbances.	Needs bandwidth tuning and good current regulation.
H_∞	[13]	Provides formal robustness. Handles disturbances well.	High order and tuning effort. It Can be hard to implement in real time.
μ-synthesis	[12]	Handles structured uncertainty. Offers robust performance margins.	Heavy design and computation. Controller can be complex.
Sliding mode	[9]	Strong robustness. Fast transients.	Chattering may appear. Increases speed ripple.
Current control			
ARC *(used)*	[16]	Uses online parameter estimates. Robust term limits ripple at high temperatures.	More involved design and tuning than fixed PI; requires accurate parameter estimates.
IMC	[17]	Simple robust shaping. Attenuates lumped disturbances.	Compensates parameter variation via disturbance rejection; no parameter estimation or update, so mismatch can remain under the temperature changes.
MFPCC	[20]	Quick response. Can handle constraints.	Same as IMC. Relies on online disturbance estimation.
Sliding mode	[18]	Robust to parameter variation. Quick transients.	Chattering raises current ripple. Needs smoothing.
Parameter estimation			
MRAS*(used)*	[27]	Online estimates from measured voltages, currents, and speed. Popov/Lyapunov support.	Needs sufficient excitation and careful tuning of the PI gains.
RLS	[24]	Lightweight and fast with good excitation.	Sensitive to noise and forgetting-factor tuning. May drift with time-varying parameters.
EKF	[25]	Explicit noise handling. Multi-parameter estimation.	Careful noise tuning needed. Higher computational load and linearization error.
Projection	[26]	Keeps estimates bounded. Prevents blow-up.	Updates are driven by the current regulation error; they may not follow slow temperature-driven parameter variations.

In these equations, u_d and u_q represent the stator voltages in the d and q axes, while i_d and i_q are the corresponding currents. The stator resistance is R_s, and L_d and L_q denote the inductances of the two axes, respectively. Here, we assume $L_d = L_q = L$ for simplicity (non-salient pole rotor). The mutual inductance between the rotor and stator is denoted by L_m. The electromagnetic torque T_e is function of the excitation rotor current i_r and stator current i_q. T_l represents the load torque, J is the rotor's inertia, and f_c is the friction coefficient. The rotor and electrical speeds are denoted by Ω and ω, related by the number of pole pairs n_p. Equation (6) describes the rotor's DC excitation, where V_r is the constant supply voltage, and R_r is the rotor resistance. To control this machine, a cascade approach is employed. The speed controller generates the reference current i_q^* while i_d^* is maintained at zero to ensure Maximum Torque per Ampere (MTPA). The current controller then provides the reference voltages u_d^* and u_q^* which are applied to the motor through a PWM inverter as shown in Fig. 1.

III. DISTURBANCE OBSERVER FOR ROTOR SPEED CONTROL

In the presence of uncertainties in the parameters of the WRSM, (4) can be rewritten as follows [34]:

$$\frac{d\Omega}{dt} = \frac{1}{J}(T_e - T_l - f_c\Omega + \delta) = k_t i_q - D_w \tag{7}$$

where δ represents the parameters uncertainties, $D_w = 1/J(f_c\Omega + T_l - \delta)$ denotes the total disturbance affecting the system, and $k_t = 1.5\, n_p L_m i_r / J$.

As in [16], it is assumed that the closed-loop transfer function between the reference speed Ω^* and the measured speed Ω is a first-order function with a time constant τ_w, then:

$$\frac{\Omega(s)}{\Omega^*(s)} = \frac{1}{(1 + \tau_w s)} \tag{8}$$

If the reference current i_q^*, which is the output of the speed controller DOBC, is used instead of i_q (assuming that i_q is regulated), then i_q^* becomes:

$$i_q^* = \frac{1}{k_t}\left(\frac{1}{\tau_w} e_w + D_w\right) \tag{9}$$

where $e_w = \Omega^* - \Omega$ is the speed control error. The disturbance D_w cannot be easily measured. Therefore, in most cases, it is estimated by an observer. As described in [15], a nonlinear system affected by disturbances, can be modeled as:

$$\frac{dx}{dt} = f(x) + g_1(x)u + g_2(x)D \tag{10}$$

where x represents the state vector, u is the control input, and D represents the total disturbance affecting the system. The functions $f(x)$, $g_1(x)$, and $g_2(x)$ are state dependent.

The disturbance term D can be estimated as follows:

$$\begin{cases} \hat{D} = z + p(x) \\ \dfrac{dz}{dt} = -l(x)\begin{bmatrix} g_2(x)z + g_2(x)p(x) \\ +f(x) + g_1(x)u \end{bmatrix} \end{cases} \tag{11}$$

where z is an internal vector, $p(x)$ is a function of x, and $l(x) = \partial p(x)/\partial x$ is the gain of the observer. According to [34], $\hat{D}$ converges if:

$$\frac{\partial p(x)}{\partial x} = \frac{\eta}{g_2(x)}, \quad \eta > 0 \tag{12}$$

By performing the identification between (7), (10), and (11), D can be estimated as follows:

$$\begin{cases} \hat{D}_w = z - \eta\Omega, \\ \dfrac{dz}{dt} = \eta\left(k_t i_q - z + \eta\Omega\right) = \eta\left(k_t i_q - \hat{D}_w\right) \end{cases} \tag{13}$$

So, i_q^* will be written using $\hat{D}_w$:

$$i_q^* = \frac{1}{k_t}\left(\frac{1}{\tau_w}e_w + \hat{D}_w\right) \tag{14}$$

Therefore, (13) and (14) act as the speed controller by generating i_q^*.

IV. MODEL REFERENCE ADAPTIVE SYSTEM (MRAS) FOR PARAMETERS ESTIMATION

MRAS is commonly applied to estimate electrical parameters and speed in rotating machines [27], [28]. In this section, we describe the implementation of the MRAS technique for estimating the WRSM parameters, including stator resistance R_s, stator inductance L, and rotor flux $\lambda_m = L_m i_r$. These estimated parameters (noted by $\hat{R}_s$, $\hat{L}$ and $\hat{\lambda}_m$ respectively) will be used for current control in the following section. The motor equations are expressed as:

$$\frac{di}{dt} = Ai + Bu + C \tag{15}$$

where $i = \begin{bmatrix} i_d \\ i_q \end{bmatrix}$, $u = \begin{bmatrix} u_d \\ u_q \end{bmatrix}$, $A = \begin{bmatrix} -\frac{R_s}{L} & \omega \\ -\omega & -\frac{R_s}{L} \end{bmatrix}$, $B = \begin{bmatrix} \frac{1}{L} & 0 \\ 0 & \frac{1}{L} \end{bmatrix}$, $C = \begin{bmatrix} 0 \\ -\frac{\omega\lambda_m}{L} \end{bmatrix}$.

The estimated current $\hat{i}$ using estimated parameters is implemented as in [27]:

$$\frac{d\hat{i}}{dt} = \hat{A}\hat{i} + \hat{B}u + \hat{C} + G(\hat{i} - i) \tag{16}$$

where $\hat{A} = \begin{bmatrix} -\frac{\hat{R}_s}{\hat{L}} & \omega \\ -\omega & -\frac{\hat{R}_s}{\hat{L}} \end{bmatrix}$, $\hat{B} = \begin{bmatrix} \frac{1}{\hat{L}} & 0 \\ 0 & \frac{1}{\hat{L}} \end{bmatrix}$, $\hat{C} = \begin{bmatrix} 0 \\ -\frac{\omega\hat{\lambda}_m}{\hat{L}} \end{bmatrix}$, $G = \begin{bmatrix} K_1 & 0 \\ 0 & K_2 \end{bmatrix}$, $K_1, K_2 > 0$.

Assuming $\hat{e} = \left[i - \hat{i}\right]^T = \left[i_d - \hat{i}_d \;\; i_q - \hat{i}_q\right]^T$, we get:

$$\frac{d\hat{e}}{dt} = (A + G)\hat{e} + w \tag{17}$$

where $w = (A - \hat{A})\hat{i} + (B - \hat{B})u + (C - \hat{C})$. Supposing $a = R_s/L$, $b = 1/L$, $c = \lambda_m/L$ and w can be written as:

$$w = \begin{bmatrix} -\hat{i}_d & u_d & 0 \\ -\hat{i}_q & u_q & -\omega \end{bmatrix}\begin{bmatrix} a - \hat{a} \\ b - \hat{b} \\ c - \hat{c} \end{bmatrix} = \Gamma \cdot \Delta_\psi \tag{18}$$

where $\Gamma = \begin{bmatrix} -\hat{i}_d & u_d & 0 \\ -\hat{i}_q & u_q & -\omega \end{bmatrix}$ and $\Delta_\psi = \begin{bmatrix} a - \hat{a} \\ b - \hat{b} \\ c - \hat{c} \end{bmatrix}$.

According to [34], to ensure stability, the following two conditions must be met:

1) The nonlinear feedback term satisfies the Popov integral inequality:

$$\int_0^t w^T \hat{e} d\tau \geq -\gamma_0^2, \quad \gamma_0 > 0 \tag{19}$$

2) The linear component matrix $(A + G)$ must be strictly positive definite, which requires $K_1, K_2 \leq R_s/L$.

Based on these two conditions, the estimation equations for the parameters are derived as described in [27]:

$$\begin{cases} \hat{a} &= \hat{a}(0) - \left(K_{f2} + \dfrac{K_{f1}}{s}\right)(\hat{i}_d\hat{e}_d + \hat{i}_q\hat{e}_q) \\ \hat{b} &= \hat{b}(0) + \left(K_{g2} + \dfrac{K_{g1}}{s}\right)(u_d\hat{e}_d + u_q\hat{e}_q) \\ \hat{c} &= \hat{c}(0) - \left(K_{h2} + \dfrac{K_{h1}}{s}\right)(\omega\hat{e}_q) \end{cases} \tag{20}$$

where $\hat{e}_d = \hat{i}_d - i_d$, $\hat{e}_q = \hat{i}_q - i_q$, and $K_{(f,g,h)1}$ and $K_{(f,g,h)2}$ are the coefficients of the PI controllers.

Based on [32], [33], if the two above conditions are satisfied, then we get:

$$\lim_{t\to\infty} \hat{e}(t) = 0 \quad \text{and} \quad \lim_{t\to\infty} \Delta_\psi(t) = 0.$$

The transfer function relating the estimated parameters $\hat{a}, \hat{b}, \hat{c}$ and Δ_ψ is established to facilitate the appropriate selection of the gain coefficients $K_{(f,g,h)1}$ and $K_{(f,g,h)2}$ [34]. In practice, MRAS uses low-pass filter in current and speed measurements to attenuate noise and ripple, and the adaptation PIs include anti-windup to prevent integrator windup issues and keep the parameter estimates within prescribed bounds. To conclude, the WRSM parameters can be effectively estimated using the MRAS approach, as formulated in (16) and (20).

V. ADAPTIVE ROBUST CONTROL FOR WRSM CURRENTS REGULATION

From (1) and (2), the electrical equation of the WRSM can be written as follows:

$$\begin{cases} L\dfrac{di_d}{dt} &= \phi_d\psi_d + u_d \\ L\dfrac{di_q}{dt} &= \phi_q\psi_q + u_q \end{cases} \tag{21}$$

where

$$\phi_q = \begin{bmatrix} -i_q & -\omega i_d & -\omega \end{bmatrix}, \quad \phi_d = \begin{bmatrix} -i_d & \omega i_q \end{bmatrix},$$
$$\psi_q = \begin{bmatrix} R_s & L & \lambda_m \end{bmatrix}^T, \quad \psi_d = \begin{bmatrix} R_s & L \end{bmatrix}^T.$$

Considering the state vector $X = \begin{bmatrix} i_d & i_q \end{bmatrix}^T$. With parameter variations, (21) can be rewritten as:

$$L\frac{dX}{dt} = \phi\psi + u + \Delta \tag{22}$$

where $\phi = \begin{bmatrix} -i_d & \omega i_q & 0 & 0 & 0 \\ 0 & 0 & -i_q & -\omega i_d & -\omega \end{bmatrix}$, $\psi = \begin{bmatrix} \psi_d & \psi_q \end{bmatrix}^T$ and $\Delta = \begin{bmatrix} \Delta_d & \Delta_q \end{bmatrix}^T$ represents the parameters fluctuations and external disturbances.

The control law consists of two reference voltage components [16]:

- **Adaptive component** u_a: designed under the assumption of no external disturbances ($\Delta = 0$). This term compensates for the parameter variations of the machine that occur mainly due to temperature changes.
- **Robust component** u_f: introduced to explicitly compensate for both the dynamic effects of parameter uncertainties and possible external disturbances ($\Delta \neq 0$).

Without external disturbances ($\Delta = \mathbf{0}$), the adaptive component u_a can be expressed as:

$$u_a = L\frac{dX^*}{dt} - \phi\hat{\psi} - k(X - X^*), \qquad k > 0 \tag{23}$$

where X^* is the reference current vector, $\hat{\psi}$ represents the estimated parameters obtained from the MRAS observer described in the previous section, and $e = X - X^*$ is the current regulation error.
By replacing (23) in (22), the following equation is obtained:

$$L\frac{de}{dt} + ke = -\phi(\hat{\psi} - \psi) = -\phi e_\psi \tag{24}$$

where $e_\psi = \hat{\psi} - \psi$ represents the error in parameters estimation.

Without external disturbances ($\Delta \neq= 0$), u_f is defined as:

$$u_f = -h\,\mathrm{sgn}(e) \tag{25}$$

where $h = |\phi||\hat{\psi}_{\max} - \hat{\psi}_{\min}| + |\Delta|$, $\hat{\psi}_{\max}$ and $\hat{\psi}_{\min}$ represent the maximum and minimum values of $\hat{\psi}$, respectively. It is also assumed that both ψ and $\hat{\psi}$ belong to the interval $[\hat{\psi}_{\min}, \hat{\psi}_{\max}]$, which implies $|e_\psi| \leq |\hat{\psi}_{\max} - \hat{\psi}_{\min}|$. Finally, the reference voltage u^* applied to the machine is obtained as the sum of the two control components, adaptive and robust:

$$u^* = \begin{bmatrix} u_d^* \\ u_q^* \end{bmatrix} = u_a + u_f$$
$$= L\frac{dX^*}{dt} - \phi\,\hat{\psi} - k\,e - h\,\mathrm{sgn}(e) \tag{26}$$

The Lyapunov approach will be applied to prove the stability in both cases. for u_a, an energy function ξ_a including the regulation error e as well as the estimation errors $\hat{e}$ and e_ψ is used:

$$\xi_a = \frac{1}{2}Le^2 + \frac{1}{2}\hat{e}^2 + \frac{1}{2}e_\psi^2 \geq 0 \tag{27}$$

To prove stability, ξ_a must be positive, which is the case, and its derivative over time should be negative.

$$\frac{d\xi_a}{dt} = L\frac{de}{dt}\cdot e + \hat{e}\left[(A+G)\hat{e} + w\right] + e_\psi\frac{de_\psi}{dt}$$
$$= -\phi e_\psi e - ke^2 + \hat{e}\left[(A+G)\hat{e} + w\right] + e_\psi\frac{de_\psi}{dt} \tag{28}$$

From the previous section, $(A+G)\hat{e}^2$ is a negative value and $\lim_{t\to\infty}\Delta_\psi(t) = 0$, which implies $\lim_{t\to\infty} e_\psi(t) = 0$. Therefore, this derivative can be approximated as:

$$\frac{d\xi_a}{dt} \approx -ke^2 + (A+G)\hat{e}^2 \leq 0 \tag{29}$$

Now, a different energy function V_f is considered to demonstrate the stability of u_f:.

$$\xi_f = \frac{1}{2}Le^2 \geq 0 \tag{30}$$

$$\frac{d\xi_f}{dt} = e(-ke + u_f - \phi e_\psi + \Delta)$$
$$\leq -ke^2 + |e|\left(-h + |\phi e_\psi + \Delta|\right)$$
$$\leq -ke^2 \leq 0 \tag{31}$$

Thus, (26) will be used as the current regulator to generate the voltage u^*, which accounts for all parameter cases (with or without variations). To avoid measurement noise, i_d, i_q, and ω are set to their reference values, and $h \times \mathrm{sgn}(e)$ is replaced by $1/(4\epsilon)h^2 e$, where ϵ is a small positive constant. The block diagram of this control law is presented in Fig. 1.

VI. SIMULATION RESULTS

To validate the control method, MATLAB/Simulink simulations are conducted, and performance is compared with the IMC robust control method [8] and the FOC method [36]. The test starts under no-load conditions with constant parameters: the no-load torque T_{l0} is fixed at the experimentally measured value 4.7 N · m to account for mechanical losses. After the initial no-load phase, the total load torque T_l (including T_{l0}) is applied.

In the simulations, the machine equations (1)–(6) are used with temperature-dependent parameters: $R_s = R_s(T_s)$ and $R_r = R_r(T_r)$ as in (32), where T_s and T_r are the stator and rotor temperatures respectively. The rotor flux is taken as $\lambda_m(T_r) = L_m\, i_r(T_r)$; under constant field voltage, $i_r(T_r) = V_r/R_r(T_r)$ so that $\lambda_m(T_r)$ decreases as T_r increases. The inductances L_d, L_q (and L_m) are treated as weakly temperature dependent and are kept constant in this study.

To simulate significant operational stress, the following assumptions are considered:

1) During the first $0.1h$ (no-load), the motor parameters are assumed constant.

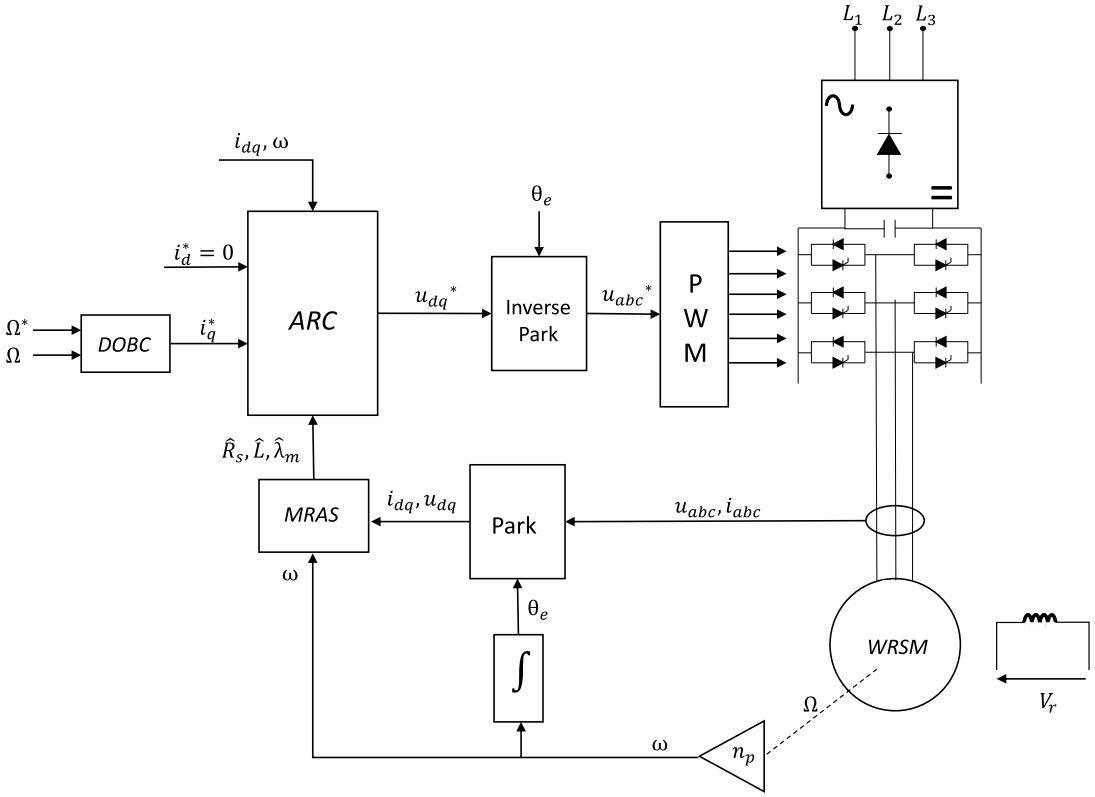

FIGURE 1. Overall block diagram of the proposed control scheme with MRAS integrated into the ARC current loop.

2) From 0.1 to $2h$ (with load), the stator and rotor resistances vary with temperature according to (32):

$$\begin{cases} R_s(T_s) = R_{s0}(1 + \alpha_{Al}(T_s - T_0)) \\ R_r(T_r) = R_{r0}(1 + \alpha_{Al}(T_r - T_0)) \end{cases} \tag{32}$$

where $\alpha_{Al} = 0.0042/°\text{C}$ is the aluminum thermal coefficient, $T_0 = 20°\text{C}$ is ambient temperature, and R_{s0}, R_{r0} are the ambient-temperature resistances values. Temperature variations $T_s(t)$ and $T_r(t)$ are modeled as first-order dynamics that fits with experimental behaviour.

3) After $2h$ both resistances stabilize as temperatures reach steady state and remain constant for approximately one hour.
4) Starting from the third hour, forced cooling is applied; $T_s(t)$ and $T_r(t)$ then decay toward ambient, and $R_s(T_s)$ and $\lambda_m(T_r)$ gradually return to their initial values over the following two hours.

An operating point is considered with the reference speed set to $\Omega^\star = 1000$ rpm and the load torque to $T_l = 12.6\ \text{N} \cdot \text{m}$. At this load, the maximum winding temperatures (measured experimentally) of the stator and rotor windings are respectively $T_{s,\max} = 164°\text{C}$ and $T_{r,\max} = 293°\text{C}$. The rotor field is supplied with a constant 43.2 V (DC), yielding an initial field current of $i_r = 16$ A at ambient temperature. The WRSM parameters at ambient temperature and at $(T_{s,\max}, T_{r,\max})$ are summarized in Table 2.

TABLE 2. The studied WRSM's parameters in cold and hot conditions.

Parameter (Unit)	Cold (T_0)	Hot ($T_{s,max}, T_{r,max}$)
R_s (ohm)	0.06	0.095
L (μH)	800	800
J (kg·m^2)	0.0013	0.0013
R_r (ohm)	2.7	5.1
λ_m (Wb)	0.067	0.031

Fig. 2 illustrates the actual values of the machine's electrical parameters with their estimates provided by MRAS. The results show that the estimated values remain stable and accurate and they will be used for current control.

Fig. 3a and Fig. 3b show the rotor speed and the electromagnetic torque respectively. The results clearly show that the proposed method significantly improves the dynamics response when the load torque is applied at time $t = 0.1$ hours comparing to the IMC and FOC at both speed and electromagnetic torque. From three to five hours, the speed regulation is notably more robust in the DOBC and IMC approach compared to FOC, exhibiting fewer ripples. This improvement is attributed to the reduction in rotor flux during this phase, which is compensated in the estimation of $\hat{D}_w$ in DOBC (14) and the robust feedback compensation in IMC [8].

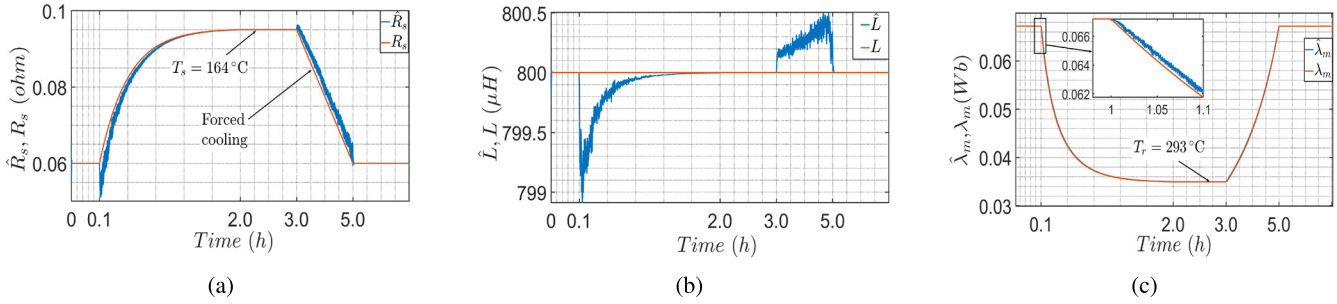

FIGURE 2. Simulation results by MRAS of estimated and actual value of: (a) stator resistance R_s (b) stator inductance L and (c) sotor flux λ_m.

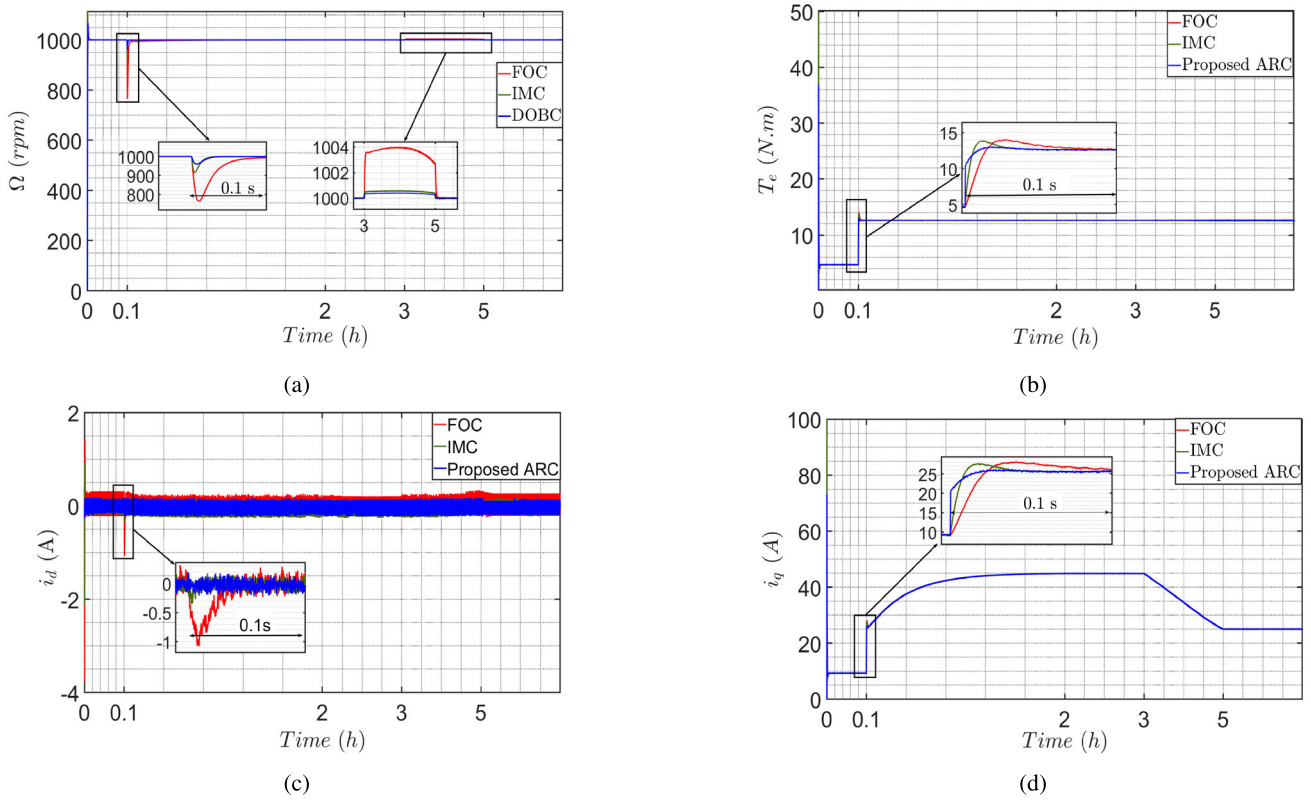

FIGURE 3. Simulation results of (a) rotor speed, (b) electromagnetic torque, (c) i_d current and (d) i_q current.

The currents i_d and i_q are shown in Fig. 3c and Fig. 3d, respectively. An improvement in dynamic response is observed with the proposed ARC and IMC method when the load torque is applied with lower undershoot with IMC and almost no undershoot with ARC. The oscillations in i_d are also reduced in the two robust methods compared to the FOC over the entire duration.

VII. EXPERIMENTAL RESULTS

The test bench shown in Fig. 4 includes a 40 kW, 4000 rpm wound rotor synchronous machine with anodized aluminum tape windings. This setup is used to validate the proposed control method. The synchronous machine is coupled to a DC machine, which acts as a generator connected to a resistive load. The control is implemented using MATLAB/Simulink and ControlDesk, via the dSpace MicroLabBox interface. Additionally, the synchronous machine is equipped with thermocouples to measure temperatures at various points,

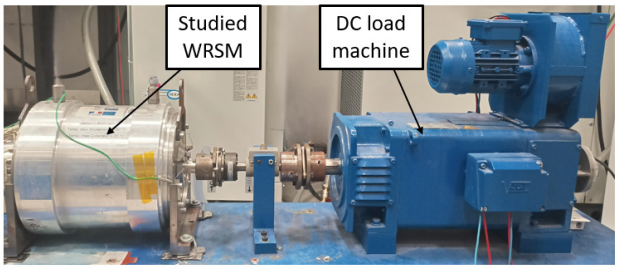

FIGURE 4. The tested wound rotor synchronous machine paired with the DC load machine.

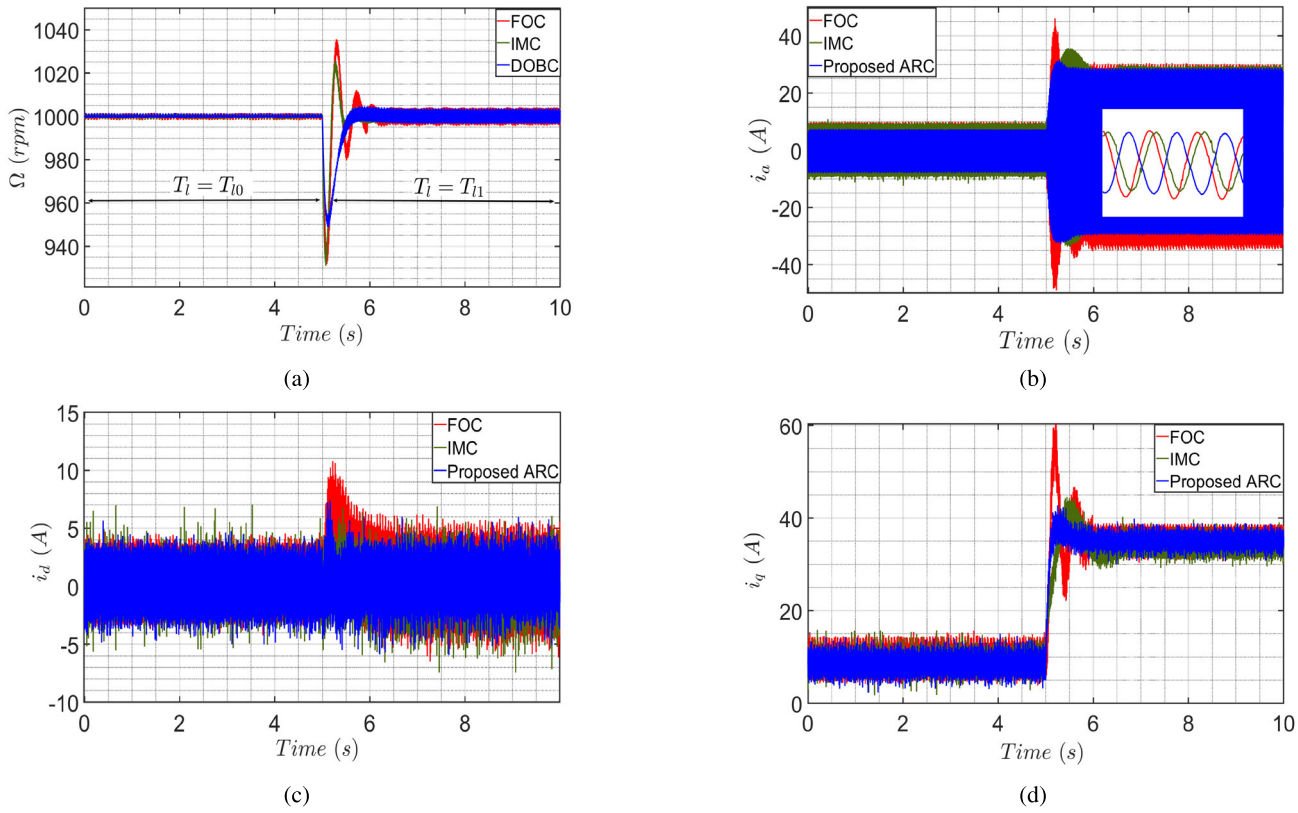

FIGURE 5. Measured value of: (a) rotor speed, (b) phase current i_a, (c) i_d current and (d) i_q current when the machine is cold at load torque T_{l1}.

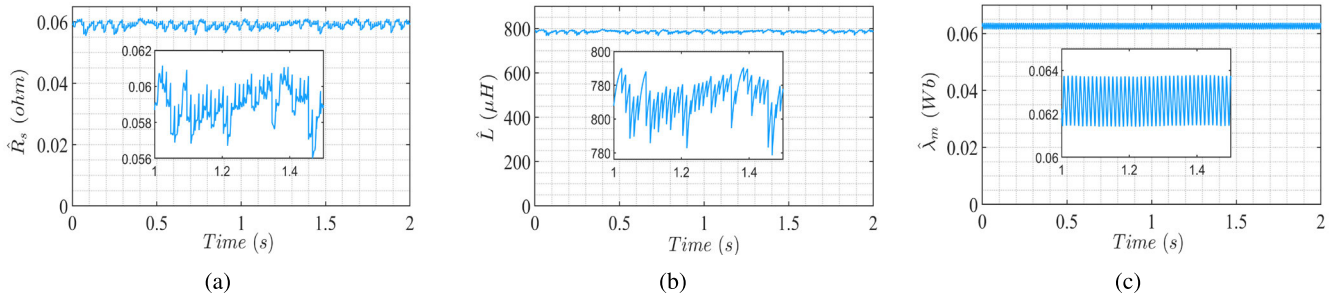

FIGURE 6. Experimental results of the estimation of: (a) stator resistance, (b) stator inductance and (c) rotor flux when the machine is cold at load torque T_{l1}.

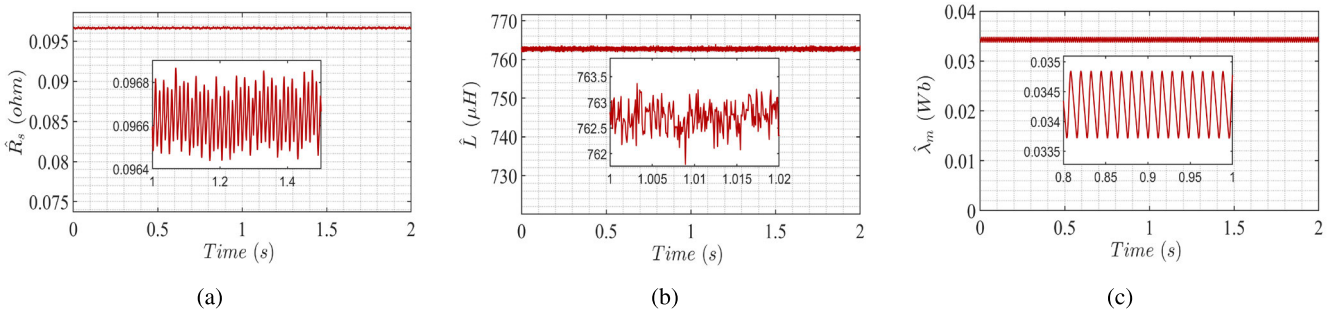

FIGURE 7. Experimental results of the estimation of: (a) stator resistance, (b) stator inductance and (c) rotor flux when the machine is hot at load torque T_{l1}.

such as stator and rotor windings. The proposed method is compared with IMC and FOC approaches.

The same operating point from the simulation of the previous section was then tested experimentally with

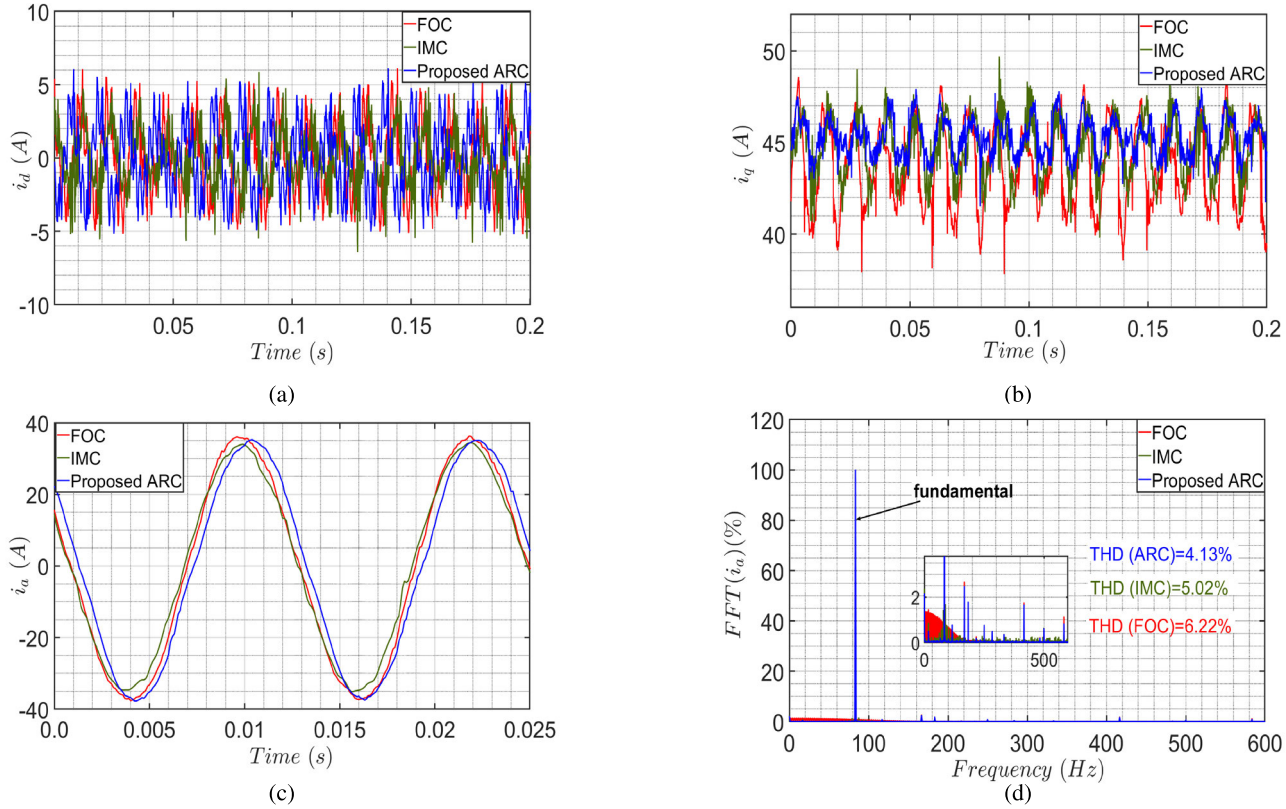

FIGURE 8. Measured value of: (a) i_d current, (b) i_q current, (c) phase current i_a, and (d) its spectrum relative to the fundamental when the machine is hot at load torque T_{l1}.

$\Omega^* = 1000\ rpm$ (Test 1). The no-load torque is estimated to 4.7 N · m. A load torque of 7.9 N · m was then added, giving a total torque of $T_{l1} = 12.6$ N · m. The speed controller parameters were selected to achieve almost the same response time for the three methods.

Fig. 5 illustrates the rotor speed when the load is applied at 5 seconds. It can be observed that the DOBC method improves system dynamics. The speed reaches the reference without overshoot and settles fastest. IMC shows a small overshoot; FOC has the largest overshoot and ripple. Both robust controllers reduce speed oscillations versus FOC. For the currents, the overshoot of i_a, i_d, and i_q is lower with the proposed controller. With FOC, i_d shows slightly more oscillations. In steady state, the i_q ripple is almost the same for the proposed ARC and IMC, and higher with FOC.

Additionally, Fig. 6 presents the parameters estimation using currents control, at the time when the load is applied and the machine is still cold, employing the MRAS method. The estimated parameters are accurate and consistent with those listed in Table 2, validating the reliability of the MRAS based estimation approach under cold operating conditions.

After approximately 75 minutes of operation at the same load point, the rotor-field winding temperature reached $T_{r,max} = 293°C$ and the stator-coil temperature reached $T_{s,max} = 164°C$ as in the simulation. It can be observed in Fig. 7 that the stator resistance increased significantly from 0.06 to 0.09 ohm, while the rotor flux decreased by nearly 50%. The estimated inductance remains almost constant, around 763 μH which confirms the assumption made in the simulation.

Fig. 8 shows the measured current i_d, i_q and i_a under these high-temperatures which are considered almost the same for the three methods. It can be observed that the i_d current maintains relatively stable oscillation levels. In contrast, the i_q current exhibits fewer oscillations with the proposed ARC method than IMC and FOC. This increase in i_q oscillations directly affects the phase currents i_a, leading to greater distortion and a rise in its total harmonic distortion (THD), which is 6.22% for the FOC, 5.02% for the IMC and 4.13% for the proposed method. Compared with the proposed ARC and IMC, FOC is the least effective under these conditions. IMC sits in between: it improves over FOC by estimating lumped disturbances, but it does not update the machine parameters, and is thus more sensitive to temperatures variation. In contrast, ARC is fed with online MRAS parameter estimates and uses a robust term for the residual mismatch, which better compensates the variations, reduces oscillations, and improves overall current quality.

To evaluate the performance of the proposed method in low-speed applications, a second operating point is set at $\Omega^* = 400\ rpm$ with almost the same load torque

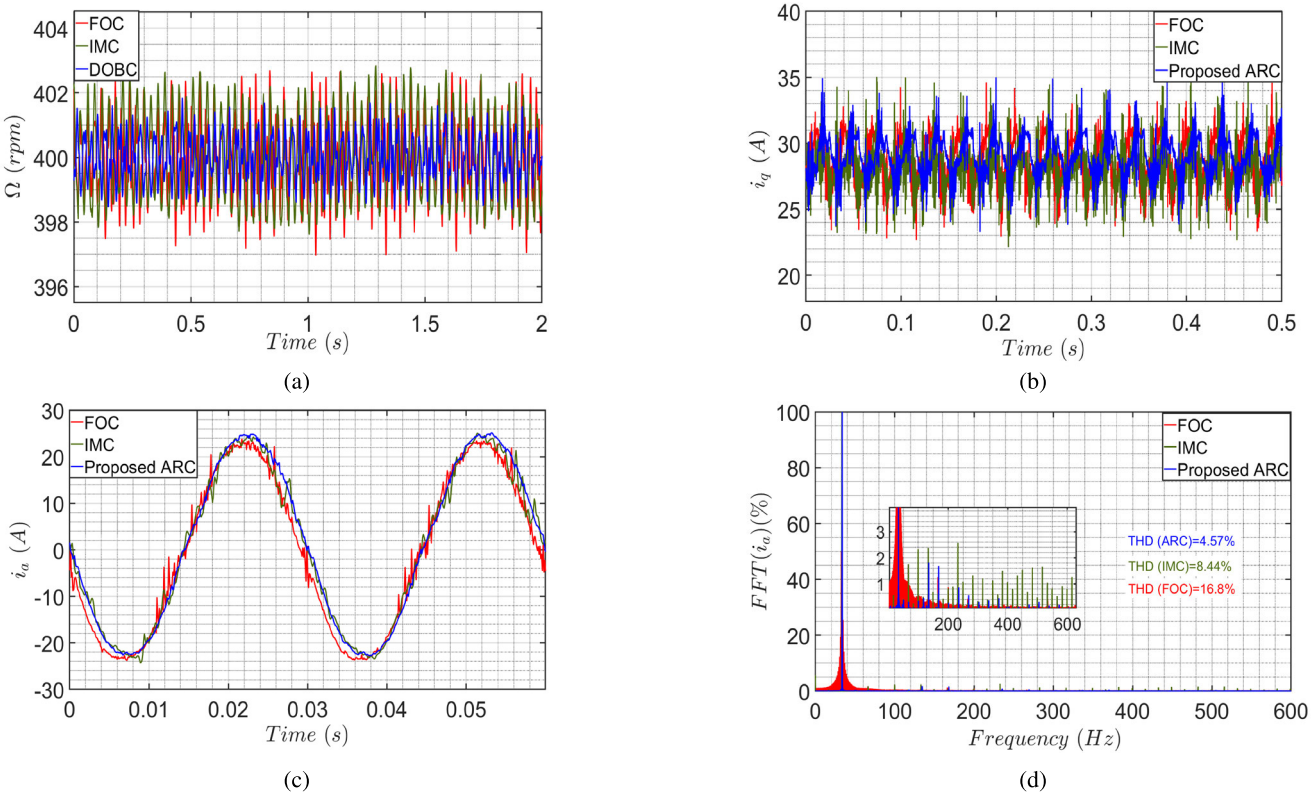

FIGURE 9. Measured value of: (a) rotor speed, (b) i_q current, (c) Phase current i_a, and (d) its spectrum relative to the fundamental when the machine is hot at 400 rpm.

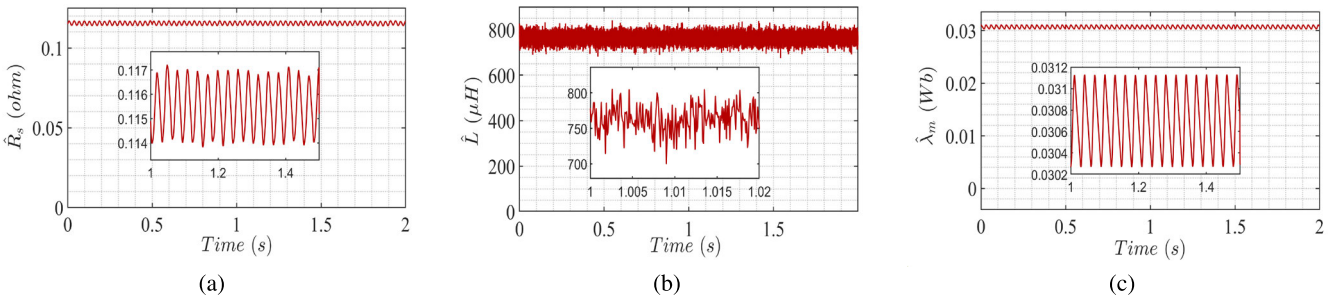

FIGURE 10. Experimental results of the estimation of: (a) stator resistance, (b) stator inductance, and (c) rotor flux when the machine is hot at 400 rpm.

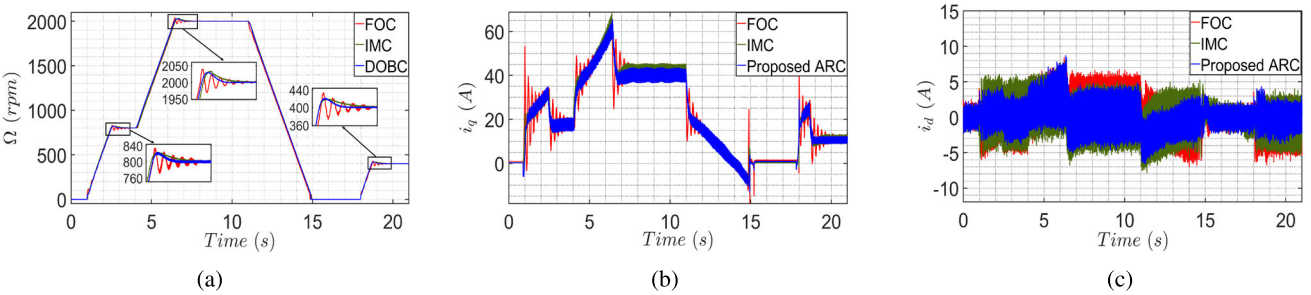

FIGURE 11. Measured value of: (a) rotor speed, (b) i_q current and (c) i_d current under benchmark test.

(Test 2). In this operating condition, the temperature stabilizes at 163°C for the stator and 286°C for the rotor. Fig. 9 shows the measured rotor speed, the phase and the quadrature currents. It can be observed that the rotor velocity exhibits fewer oscillations when the DOBC and ARC are used. Similarly, the phase current i_a shows a noticeable difference

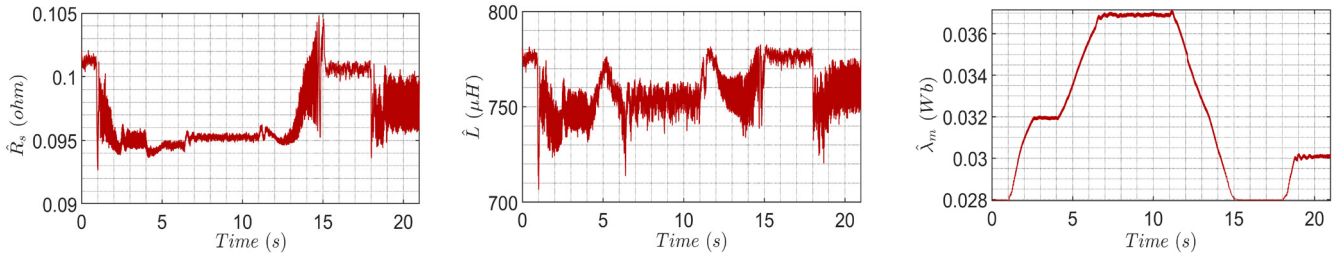

FIGURE 12. Experimental results of the estimation of: (a) stator resistance, (b) stator inductance and (c) rotor flux under benchmark test.

TABLE 3. Simulation and experimental comparison of FOC, IMC, and proposed ARC (with DOBC).

Test	Metric	FOC	IMC	Proposed ARC
SIMULATION				
Load step at 1000 rpm (ambient temperature, at $t = 0.1$ h)	Speed first undershoot (%)	23.45	8.46	4.02
	i_q overshoot (%)	11.77	7.97	1.68
	i_d undershoot (A)	1.7	0.33	0.17
cooling behavior (between 3 and 5 h)	Speed steady state error (%)	3.92	0.6	0.4
	Max torque ripple ($N.m$)	0.27	0.2	0.19
EXPERIMENTAL — Test 1 ($\Omega^* = 1000rpm$: load at $t = 5s$; cold → hot)				
Load step at $t = 5s$ (ambient temperature))	Speed first undershoot (%)	6.82	6.89	5.12
	i_d first overshoot (A)	10.7	7.51	7.32
	i_q first overshoot (%)	70.22	25.84	20.67
	i_d ripple (A) after the load	10.45	10.25	10.1
	i_q ripple (A) after the load	7.97	6.84	5.1
High temperatures ($T_s \approx 164^\circ$C, $T_r \approx 293^\circ$C)	i_d ripple (A)	10.68	10.63	10.13
	i_q ripple (A)	9.97	7.78	5.5
	THD_{i_a} (%)	6.22	5.02	4.13
EXPERIMENTAL — Test 2 (high temperature, $\Omega^* = 400rpm$)				
High temperatures ($T_s \approx 163^\circ$C, $T_r \approx 286^\circ$C)	Speed ripple (rpm)	5.73	4.71	2.87
	THD_{i_a} (%)	16.8	8.44	4.57
EXPERIMENTAL — Test 3 (Benchmark test under initial load)				
Benchmark sequence: $0 \rightarrow 800 \rightarrow 2000 \rightarrow 0 \rightarrow 400$ rpm High temperatures ($T_s \approx 169^\circ$C, $T_r \approx 295^\circ$C)	Max speed overshoot (%)	7.75	4.5	4.5
	Max i_q overshoot (A) (at $t = 15\ s$)	23	6	1.6
	Max speed ripple (rpm)	5.4	4.02	5.1
	Max i_d ripple (A)	9.31	8.74	7.9
	Max i_q ripple (A)	7.25	7.52	7.18
EXPERIMENTAL — Test 4 (Speed reversal under load)				
Speed inversion from 1000 rpm to -1000 rpm at $t = 5\ s$ High temperatures ($T_s \approx 169^\circ$C, $T_r \approx 295^\circ$C)	Speed undershoot (%)	12.13	8.8	6.6
	Speed ripple (rpm)	6.2	8.5	5.7
	i_q overershoot (A)	115	23	22.7
	i_d ripple (A)	9.5	9.8	8.34

in the spectral analysis presented in Fig. 9d, with a THD of 4.57% for the ARC method compared to 8.44% for the IMC and 16.8% for the FOC method. This reduction in current oscillations with the proposed method positively impacts the torque, reducing its fluctuations and contributing to a smoother and quieter machine operation.

Fig. 10 presents the parameter estimations after the machine was fully heated. A slight variation in inductance is observed, while the flux estimation remains accurate. However, the resistance is slightly overestimated, reaching 0.095 Ohm when applying (32), compared to its estimation, which is 0.115 ohm. A comparison of the simulation and experimental results of the three methods is provided in Table 3.

Finally, to test also the dynamics at high temperature conditions, a simplified benchmark was carried out with

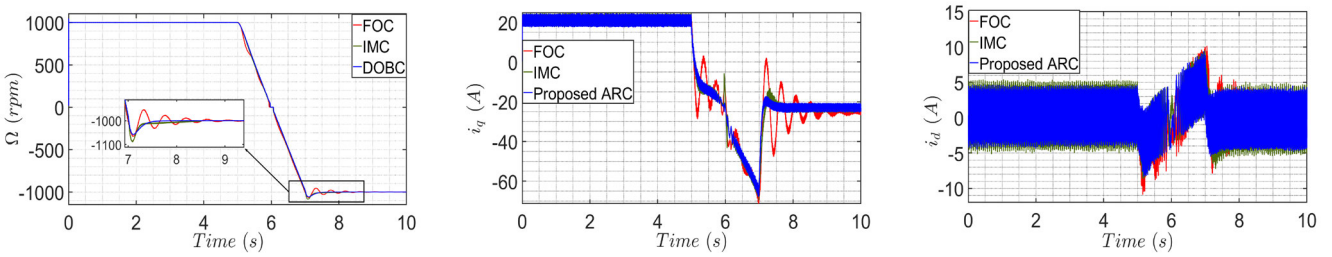

FIGURE 13. Measured value of: (a) rotor speed, (b) i_q current and (c) i_d current under speed reversal test.

$T_{r,max} = 295°C$ and $T_{s,max} = 169°C$ wich are considered the same for the three methods (Test 3): with the load applied from the start. The speed reference was set through the sequence of velocities using a rate-limited ramp as shown in Fig. 11. Under the benchmark transients, the speed response with the proposed method and with IMC shows no visible oscillations. For the i_q current, a clear overshoot and transient oscillations are produced by FOC, whereas ARC and IMC exhibit nearly the same response. For i_d, a ripple reduction is observed with the proposed ARC. During this benchmark, the MRAS parameter estimates remain consistent and accurate at this temperatures as presented in Fig. 12, they stay stable across ramps and reversals. Another test include speed reversal from $+1000$ to -1000 *rpm* (Test 4) with applied load is shown in Fig. 13. During the reversal, speed oscillations were not observed with IMC or DOBC, unlike with FOC; overshoot was also smaller with DOBC. During the transition (between 5 and 7 s), FOC showed larger oscillations in i_q, and a slight reduction in i_d ripple is achieved with the proposed ARC compared with IMC and FOC.

VIII. CONCLUSION

This paper presents a robust adaptive control scheme for a WRSM with anodized aluminum tape windings. A Model-Reference Adaptive System (MRAS) estimates the temperature-dependent parameters online, and these estimates are used by the Adaptive Robust Control (ARC) in the current loop, while a disturbance-observer-based controller (DOBC) regulates rotor speed and provides the $i_q^\star$ reference. The proposed method is compared with an Internal Model Control (IMC) strategy from the literature, used as a robust baseline, and with classical FOC-PI. Simulations under varied operating conditions with temperature-dependent parameters, together with experiments across wide temperature ranges, show that proposed ARC with DOBC improve dynamic response, reduces speed and current ripple, and decreases current THD, especially at high temperatures. By updating machine parameters online, MRAS supplies ARC with Accurate online parameter estimates; IMC mitigates lumped disturbances but, without parameter adaptation, it is more sensitive to thermal changes, and FOC is the most affected. Overall, the proposed controller provides robust, high-quality current regulation for WRSM operation under varying thermal conditions.

NOMENCLATURE

R_s	Stator resistance.
L	Stator inductance.
R_r	Rotor resistance.
λ_m	Rotor flux.
J	Rotor inertia.
i_d, i_q	Direct and quadrature current.
u_d, u_q	Direct and quadrature tension.
Ω	Rotor speed.
ω	Electrical speed.
D_w	Total disturbance of the rotor motion.
e_w	Rotor speed regulation error.
$\hat{i}_d$, $\hat{i}_q$	Estimated currents.
$\hat{e}$	Estimation current error.
e	Regulation current error.
ψ, $\hat{\psi}$	WRSM's parameter matrix and its estimate.
e_ψ	Estimation parameters error.
ξ_a, ξ_f	Energy functions.
T_0	Ambient temperature.
$T_{s,max}$	Maximum stator temperature.
$T_{r,max}$	Maximum rotor temperature.

ACKNOWLEDGMENT

This work has been achieved within the framework of EE4.0 project (Energie Electrique 4.0). EE4.0 is co-financed by European Union with the financial support of the European Regional Development Fund (ERDF), French State and the French Region of Hauts-de-France.

REFERENCES

[1] P. Haghgooei, A. Corne, E. Jamshidpour, N. Takorabet, D. A. Khaburi and B. Nahid-Mobarakeh, "Current sensorless control for a wound rotor synchronous machine based on flux linkage model," *IEEE J. Emerg. Sel. Topics Power Electron.*, vol. 10, no. 4, pp. 4576–4586, Aug. 2022, doi: 10.1109/JESTPE.2021.3121135.

[2] R. Cousseau, R. Romary, F. Balavoine, M. Irhoumah, and R. Pusca, "Comparative study of permanent magnet synchronous machine vs salient pole synchronous machine in high temperature application," *Eur. Phys. J. Appl. Phys.*, vol. 97, p. 52, 2022.

[3] S. Ayat, R. Wrobel, J. Baker, and D. Drury, "A comparative study between aluminium and copper windings for a modular-wound IPM electric machine," in *Proc. IEEE Int. Electric Mach. Drives Conf. (IEMDC)*, May 2017, pp. 1–8.
[4] R. Wrobel, D. Salt, N. Simpson, and P. H. Mellor, "Comparative study of copper and aluminium conductors–future cost effective PM machines," in *Proc. 7th IET Int. Conf. Power Electron., Mach. Drives (PEMD)*, Apr. 2014, pp. 1–6.
[5] S. Babicz, S. Ait-Amar, G. Velu, A. Cavallini, and P. Mancinelli, "Behavior of anodized aluminum strip under sine and square wave voltage," *IEEE Trans. Dielectr. Electr. Insul.*, vol. 24, no. 1, pp. 39–46, Feb. 2017.
[6] A. Balamurali, A. K. Anik, W. Clandfield, and N. C. Kar, "Non-invasive parameter and loss determination in PMSM considering the effects of saturation, cross-saturation, time harmonics, and temperature variations," *IEEE Trans. Magn.*, vol. 57, no. 2, pp. 1–6, Feb. 2021.
[7] O. Bilgin and F. A. Kazan, "The effect of magnet temperature on speed, current and torque in PMSMs," in *Proc. 22nd Int. Conf. Electr. Mach. (ICEM)*, Sep. 2016, pp. 2080–2085.
[8] X. Fu, H. He, Y. Xu, and X. Fu, "A strongly robust and easy-tuned current controller for PMSM considering parameters variation," *IEEE Access*, vol. 8, pp. 44228–44238, 2020.
[9] K. Li, J. Ding, X. Sun, and X. Tian, "Overview of sliding mode control technology for permanent magnet synchronous motor system," *IEEE Access*, vol. 12, pp. 71685–71704, 2024.
[10] R. Errouissi, A. Al-Durra, S. M. Muyeen, and S. Leng, "Continuous-time model predictive control of a permanent magnet synchronous motor drive with disturbance decoupling," *IET Electric Power Appl.*, vol. 11, no. 5, pp. 697–706, May 2017.
[11] H. Hamad Boughezala, K. Laroussi, S. Khadar, A. Saad Al-Sumaiti, and M. A. Mossa, "Optimized sensorless control of five-phase permanent magnet synchronous motor using a genetic algorithm-real time implementation," *IEEE Access*, vol. 12, pp. 98367–98378, 2024.
[12] R. Cai, R. Zheng, M. Liu, and M. Li, "Robust control of PMSM using geometric model reduction and μ-synthesis," *IEEE Trans. Ind. Electron.*, vol. 65, no. 1, pp. 498–509, Jan. 2018.
[13] X. Zhao, B. Zhou, and J. Zhu, "Enhancing stability in wind energy: A robust H-infinity approach for permanent magnet synchronous generators," in *Proc. 6th Int. Conf. Power Energy Technol. (ICPET)*, Jul. 2024, pp. 504–508.
[14] E. Sariyildiz, R. Oboe, and K. Ohnishi, "Disturbance observer-based robust control and its applications: 35th anniversary overview," *IEEE Trans. Ind. Electron.*, vol. 67, no. 3, pp. 2042–2053, Mar. 2020.
[15] J. Yang, W.-H. Chen, and S. Li, "Non-linear disturbance observer-based robust control for systems with mismatched disturbances/uncertainties," *IET Control Theory Appl.*, vol. 5, no. 18, pp. 2053–2062, 2011, doi: 10.1049/iet-cta.2010.0616.
[16] J. Xia, Z. Li, D. Yu, Y. Guo, and X. Zhang, "Robust speed and current control with parametric adaptation for surface-mounted PMSM considering system perturbations," *IEEE J. Emerg. Sel. Topics Power Electron.*, vol. 9, no. 3, pp. 2807–2817, Jun. 2021.
[17] Y. Huang and S. Xiong, "IMC-based current observer for PMSM," *Electron. Lett.*, vol. 51, no. 25, pp. 2100–2102, Dec. 2015.
[18] T. Smidt Gabbi, H. A. Gründling, and R. Padilha Vieira, "Discrete-time sliding mode control based on disturbance observer applied to current control of permanent magnet synchronous motor," *IET Power Electron.*, vol. 14, no. 4, pp. 875–887, Mar. 2021.
[19] Y. Zhang, J. Jin, and L. Huang, "Model-free predictive current control of PMSM drives based on extended state observer using ultralocal model," *IEEE Trans. Ind. Electron.*, vol. 68, no. 2, pp. 993–1003, Feb. 2021.
[20] X. Yuan, Y. Zuo, Y. Fan, and C. H. T. Lee, "Model-free predictive current control of SPMSM drives using extended state observer," *IEEE Trans. Ind. Electron.*, vol. 69, no. 7, pp. 6540–6550, Jul. 2022.
[21] L. Xu, G. Chen, and Q. Li, "Cascaded speed and current model of PMSM with ultra-local model-free predictive control," *IET Electr. Power Appl.*, vol. 15, no. 11, pp. 1424–1437, Nov. 2021.
[22] C. Hu, Z. Wang, Y. Zhu, M. Zhang, and H. Liu, "Performance-oriented precision LARC tracking motion control of a magnetically levitated planar motor with comparative experiments," *IEEE Trans. Ind. Electron.*, vol. 63, no. 9, pp. 5763–5773, Sep. 2016.
[23] J. Zhang, W. Ren, and X.-M. Sun, "Current-constrained adaptive robust control for uncertain PMSM drive systems: Theory and experimentation," *IEEE Trans. Transport. Electrific.*, vol. 9, no. 3, pp. 4158–4169, Sep. 2023.
[24] M. Nachtsheim, J. Ernst, C. Endisch, and R. Kennel, "Performance of recursive least squares algorithm configurations for online parameter identification of induction machines in an automotive environment," *IEEE Trans. Transport. Electrific.*, vol. 9, no. 3, pp. 4236–4254, Sep. 2023.
[25] M. Abdelrahem, M. Abdel-Salam, I. Eid, and A. Elnozahy, "Extended Kalman filter for parameters estimation of permanent magnet synchronous generators in wind energy systems," in *Proc. 25th Int. Middle East Power Syst. Conf. (MEPCON)*, Dec. 2024, pp. 1–6.
[26] C. Hu, Z. Hu, Y. Zhu, and Z. Wang, "Advanced GTCF-LARC contouring motion controller design for an industrial X–Y linear motor stage with experimental investigation," *IEEE Trans. Ind. Electron.*, vol. 64, no. 4, pp. 3308–3318, Apr. 2017.
[27] Q. An and L. Sun, "On-line parameter identification for vector controlled PMSM drives using adaptive algorithm," in *Proc. IEEE Vehicle Power Propuls. Conf.*, Sep. 2008, pp. 1–6.
[28] M. Kumar and S. Das, "Model reference adaptive system based sensorless speed estimation of brushless doubly-fed reluctance generator for wind power application," *IET Power Electron.*, vol. 11, no. 14, pp. 2355–2366, Nov. 2018.
[29] X. Tu, X. Hou, J. Zhao, S. Yan, and Y. Xiong, "Speed identification of speed sensorless linear induction motor based on MRAS," *CES Trans. Electr. Mach. Syst.*, vol. 7, no. 3, pp. 294–300, Sep. 2023.
[30] R. Guan, J. Liu, M. Li, M. Xiao, and X. Shi, "A compensation method for PMSM sensorless control with parameter identification considering SMO observation error," *IET Electr. Power Appl.*, vol. 18, no. 12, pp. 1730–1739, Dec. 2024.
[31] K. Wróbel, G. Tarchała, K. Szabat, and S. Katsura, "Improving regenerating mode operation of MRAS-based induction motor speed estimation using the multilayer technique," *IEEE Access*, vol. 12, pp. 153063–153073, 2024.
[32] K. Narendra and L. Valavani, "A comparison of Lyapunov and hyperstability approaches to adaptive control of continuous systems," *IEEE Trans. Autom. Control*, vol. AC-25, no. 2, pp. 243–247, Apr. 1980.
[33] C. I. Byrnes and W. Lin, "Losslessness, feedback equivalence, and the global stabilization of discrete-time nonlinear systems," *IEEE Trans. Autom. Control*, vol. 39, no. 1, pp. 83–98, Jan. 1994.
[34] R. Jbayli, Y. Azzoug, R. Cousseau, R. Pusca, and R. Romary, "Disturbance observer and adaptive robust control for PMSM drive using MRAS-based parameters estimation," in *Proc. Int. Conf. Appl. Theor. Electr. (ICATE)*, 2024, pp. 1–7.
[35] R. Jbayli, Y. Azzoug, R. Cousseau, R. Pusca, and R. Romary. (Apr. 2025). *Robust Control of a High-Temperature Synchronous Machine With Anodized Aluminum Coils*. [Online]. Available: https://hal.science/hal-05061161
[36] M. Khatab, A. Nouh, and A. S. Abd-Alraheem, "A comparative study of field oriented and backstepping control strategies for wind turbine PM synchronous generator," *Int. J. Eng. Res.*, vol. 3, no. 1, pp. 13–32, 2024.

RIYAD JBAYLI was born in Tartus, Syria, in 2001. He received the Engineering Diploma degree in electrical engineering with a specialization in industrial control from Lebanese University, and the master's degree in automatic and electrical energy from the University of Poitiers, France, in 2023, as part of a double-degree program. He is currently pursuing the Ph.D. degree with the Laboratoire des Systémes Électrotechniques et Environnement (LSEE), University of Artois, France. His research interests include the control of electric machines, high-frequency modeling, and fault diagnosis of rotating machines.

YOUNES AZZOUG received the M.S. degree in renewable energy from the University of Batna, Algeria, in 2016, and the dual Ph.D. degree in electrical engineering from LGEB, University of Biskra, and LSEE, Artois University, in 2021. He has been a Lecturer-Researcher with Artois University, France, since 2022. His research interests include electrical machine diagnosis, robust control, and fault-tolerant control, aiming to enhance the reliability and performance of electrical systems.

ROMAIN COUSSEAU received the Ph.D. degree from the University of Technology of Compiègne, Compiègne, France, in 2015. He is currently a Research Engineer with the Laboratory of Electrical Systems and Environment (LSEE). His research interests include the design of an integrated machine testbench and its control.

REMUS PUSCA (Member, IEEE) was born in Mediaş, Romania, in 1972. He received the Electrical Engineering degree from the Technical University of Cluj-Napoca, in 1995, and the Ph.D. degree in electrical engineering from the University of Franche-Comté, Besançon, France, in 2002. He is currently a Full Professor and a Researcher with the Laboratory of Electrical Systems and Environment, Artois University. His research interests include the control of electrical systems and the diagnosis of electrical machines.

RAPHAEL ROMARY (Member, IEEE) received the Ph.D. degree from Lille University, Lille, France, in 1995, and the D.Sc. degree from Artois University, Béthune, France, in 2007. He is currently a Full Professor with Artois University and a Researcher with the Laboratory of Electrical Systems and Environment. His research interests include the analytical modeling of electrical machines with applications to noise and vibration, losses, and electromagnetic emissions, and diagnosis.